Tools for Image Analysis and First Wall Protection at W7-X

Fabio Pisano,[a]* Barbara Cannas,[a] Alessandra Fanni,[a] Giuliana Sias,[a] Marcin W. Jakubowski,[b] Peter Drewelow,[b] Holger Niemann,[b] Aleix Puig Sitjes,[b] Yu Gao,[c] Victor Moncada,[d] Glen Wurden[e] and W7-X Team[b,f]

[a]*University of Cagliari, Department of Electrical and Electronic Engineering, Cagliari, Italy*

[b]*Max-Planck-Institut für Plasmaphysik, Teilinstitut Greifswald, Greifswald, Germany*

[c]*Forschungszentrum Jülich GmbH, Institut für Energie- und Klimaforschung – Plasmaphysik, Jülich, Germany*

[d]*CEA, IRFM, Saint Paul lez Durance, France*

[e]*Los Alamos National Laboratory, Los Alamos, New Mexico, USA*

[f]*See the authors list in R. C. Wolf et al., Nucl. Fusion 57, 102020 (2017)*

This submission is part of the 2019 IAEA TM on Fusion Data Processing, Validation and Analysis.

Correspondence details for corresponding author:

Dr. Fabio Pisano

Department of Electrical and Electronic Engineering

University of Cagliari

Piazza D'Armi, 09123 Cagliari, Italy

Phone: +39 070 675 5898

FAX: +39 070 675 5900

*Email: fabio.pisano@diee.unica.it

Tools for Image Analysis and First Wall Protection at W7-X

Wendelstein 7-X (W7-X) is the most advanced operating stellarator in fusion research. The monitoring and control of the heat loads on the plasma facing components (PFCs) during the operation is one of the most important issues for fusion reactors, especially for W7-X which in the next operation phase should withstand heat loads of the order of 10MW/m^2 in the ten water cooled divertors. In this paper, an overview of the tools for image analysis under development at W7-X is proposed. Much emphasis is given to the problem of camera spatial calibration and scene modelling which represent the basis for the real time system under development. Some applications of these tools are also provided, with much focus on strike-line characterization.

Keywords: Image Processing, Thermography, Plasma Facing Components

I. INTRODUCTION

From the next W7-X operational campaign OP2 [Sunn Pedersen 2019], which will start at the end of 2021, ten High Heat-Flux (HHF) water-cooled divertor units will be used for power and particle exhaust, with operation times up to 30 minutes. These units are designed to withstand 10 MW/m^2 in steady state. For this fact, the need of a real time monitoring system able to detect dangerous thermal events [Puig Sitjes 2018] [Puig Sitjes 2019], analyse them automatically and choose the proper control action, is beyond any doubt. In this context, accurate and fast image analysis of infrared camera data is essential.

During the last operational campaign OP1.2, concluded in October 2018, the imaging system under development at W7-X has been tested on the analysis of IR data looking at the ten inertially–cooled test divertors. In this paper, an overview of these developments is proposed.

The paper is organized as follows. Section II gives an overview of the imaging system under development at W7-X, with a description of the thermographic diagnostics which will be used during the next operational campaign. Section III describes the camera

spatial calibration process, used to create IR camera projection models. Section IV describes two types of mapping tools used at W7-X. Section V gives an overview of the possible applications of these tools with particular attention to the strike-line characterization. Finally, in Sec. VI, the conclusions and the future work outlook are given.

II. IMAGING SYSTEM

During OP2, 10 endoscopes (IR/visible) will be used to monitor the ten divertors [Jakubowski 2018]. A real time system is under development at W7-X for the acquisition and analysis of the information coming from each endoscope. The data will be acquired, locally stored and analysed in real-time by means of a GPU. The real time system will be able to send an alarm to the interlock system in dangerous cases to stop the operation. The locally stored data will be sent through the local network for visualization and control purposes, and the detected thermal events will be stored in a thermal events database [Puig Sitjes 2019].

In the framework of data acquisition and analysis, the temperature calibration [Puig Sitjes 2018] and the calculation of the heat load distribution in the target surfaces [Gao 2019] are non-trivial problems. In fact, these calculations require knowledge about the observed materials and their emissivity, and explicit information about the position of the observed surface and the line of sight with respect to the camera eye. All this information can be taken from the scene models (see section IV.A), which contain a pixel-based segmentation of the field of view, giving information about material and spatial properties of the target surfaces. For the creation of scene models, it is necessary to build a projection model of the camera through a spatial calibration process (see section III).

Figure 1 shows an overview of the full process, starting from the raw images coming from IR cameras until the heat flux evaluation on the target surfaces. The main

inputs of the process are the raw IR images and the CAD model of the PFCs. By means of these inputs, the IR cameras are calibrated spatially, and a camera model (see section III.a) is generated. The camera model is then used to create the scene model. From the information taken from the scene model, the IR camera image, where a temperature is assigned to each pixel, is created. This image can be projected by means of the scene model on the CAD view, obtaining a surface temperature for each point in the surface. By knowing the surface temperatures, the heat flux through the surface and finally the heat flux image is calculated. From the CAD model it is also possible to create a thermal map, a CAD-based 2D map which unfolds the first wall of the stellarator (see section IV.B).

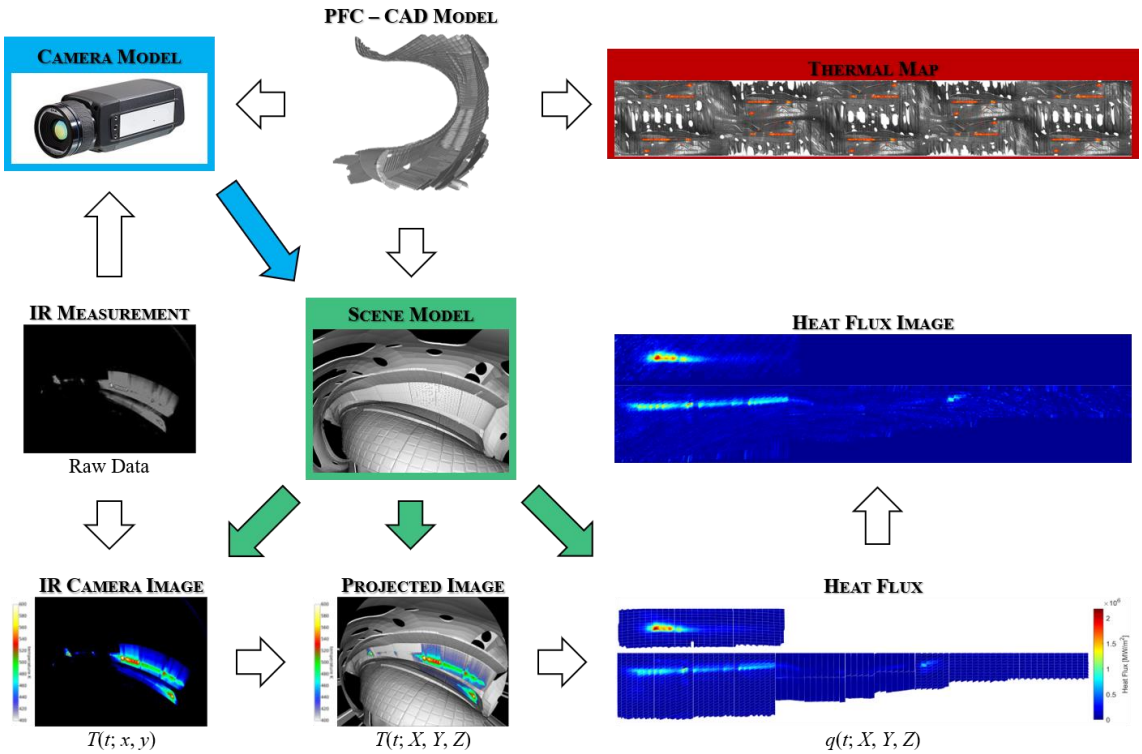

Figure 1. Overview of the imaging system, starting from raw IR measurements until temperature and heat flux calculations.

III. SPATIAL CALIBRATION

Spatial calibration is an essential phase in the all process, since it helps to build a biunivocal correspondence between the position of the pixels in the image and the actual position of the 3D points in the observed surface. In fact, this phase consists of finding a camera model, which fits as well as possible the relationship between the known 3D coordinates of a set of control points and their projection on the image plane.

III.A CAMERA MODEL

Each camera model is a pinhole model [Forsyth 2003, Sturm 2016]. Such a camera model describes the perspective of the camera as if it were an ideal pinhole camera, whose aperture is described as a point and where no lenses are used to focus light. The camera model described below is an improvement of the camera model used in [Pisano 2018], used to model cameras during the first W7-X operational campaign. The main improvement is due to the new distortion function, which helps to avoid conditioning problems in case of high distortion lenses.

The camera model depends on several parameters: extrinsic parameters, defining the pinhole position and orientation of the equivalent pinhole in the 3D world; intrinsic parameters, defining the camera focal length and skew factor in pixels and the position of the principal point in the image plane; distortion parameters, defining the lens distortion effect in terms of three components, i.e. radial, tangential and prism. Since wide angle lenses lead to large image distortions, it is very important to find a correct set of parameters.

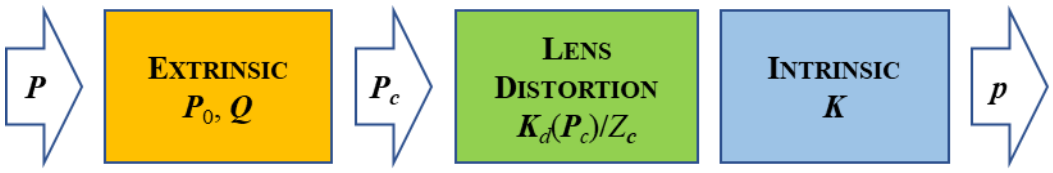

Figure 2. Projection scheme of the camera model

In the camera model, the relationship between the 3D point $\boldsymbol{P} = [X, Y, Z]$ and the pixel $\boldsymbol{p} = [x, y]$ is given by

$$\boldsymbol{p} = \frac{\boldsymbol{P}_c}{Z_c} \boldsymbol{K}_d \left(\boldsymbol{P}_c \right) \boldsymbol{K} \tag{1a}$$

where

$$\boldsymbol{P}_c = \left(\boldsymbol{P} - \boldsymbol{P}_0 \right) \boldsymbol{Q} \tag{1b}$$

In (1b), the resulting point $\boldsymbol{P}_c = [X_c, Y_c, Z_c]$ is the 3D point in the camera reference coordinate system, obtained through a translation of the 3D point $\boldsymbol{P}$ with respect to the pinhole position $\boldsymbol{P}_0$ and through a rotation by means of the camera orientation matrix $\boldsymbol{Q}$. Both $\boldsymbol{P}_0$ and $\boldsymbol{Q}$ represent the extrinsic parameters. The point $\boldsymbol{P}_c$ is then normalized in (1a) with respect to the depth coordinate Z_c, distorted by means of a distortion matrix $\boldsymbol{K}_d(\boldsymbol{P}_c)$ which models the lens distortion effect, and finally transformed into a pixel point by means of the intrinsic parameters matrix $\boldsymbol{K}$. The projection scheme is shown in Figure 2.

The distortion matrix $\boldsymbol{K}_d(\boldsymbol{P}_c) = \boldsymbol{K}_r(\boldsymbol{P}_c) + \boldsymbol{K}_{tp}(\boldsymbol{P}_c)$ in (1a) is a diagonal matrix given by the sum of two contributions: a radial distortion component $\boldsymbol{K}_r$ and a tangential-prism distortion component $\boldsymbol{K}_{tp}$.

III.B RADIAL DISTORTION

The radial distortion function has been designed in order to be general enough to deal both with immersion tubes and endoscopes used during OP1.2 experimental campaign. Moreover, it is robust enough to overcome the conditioning problems due to the state-of-the-art polynomial radial distortion models [Hughes 2008]. Moreover, these models, due to their oscillating behaviour, which is not commonly observed in lenses, overfit when interpolating and deviate completely when extrapolating.

The radial distortion matrix is given by

$$\boldsymbol{K}_r\left(\boldsymbol{P}_c\right)=\mathrm{diag}\left(f\left(\frac{R_c}{Z_c}\right),f\left(\frac{R_c}{Z_c}\right),1\right) \tag{2}$$

where $R_c=\sqrt{X_c^2+Y_c^2}$ is the radial coordinate in the camera reference system and the proposed radial distortion function is

$$\begin{gathered} f\left(r\right)=\left(1-\lambda\right)\frac{G_n\left(t_1\right)}{t_1}+\lambda\frac{G_n\left(t_2\right)}{t_2}+\begin{cases}0 & r\geq 0\\ 2\left(1-\lambda\right)r_{\gamma 1}+2\lambda r_{\gamma 2} & r<0\end{cases} \\ G_n\left(t\right)=\int_0^t\frac{1}{1+\tau^{n/2}}d\tau,\quad t_1=\frac{\left|r\right|}{r_{\gamma 1}}G_n\left(\infty\right),\quad t_2=\frac{\left|r\right|}{r_{\gamma 2}}G_n\left(\infty\right),\quad G_n\left(\infty\right)=\frac{2\pi/n}{\sin\left(2\pi/n\right)} \end{gathered} \tag{3}$$

The distortion model in (3) mainly depends on two knee points, $r_{\gamma 1}$ and $r_{\gamma 2}$, with $r_{\gamma 1}\leq r_{\gamma 2}$, and on the approximative slope λ of the distorted radius $rf(r)$ between the two knee points, as shown in Figure 3. As the parameter $n\in\mathbb{N}$ increases, the function becomes even more similar to a piecewise linear function (red dashed line in Figure 3).

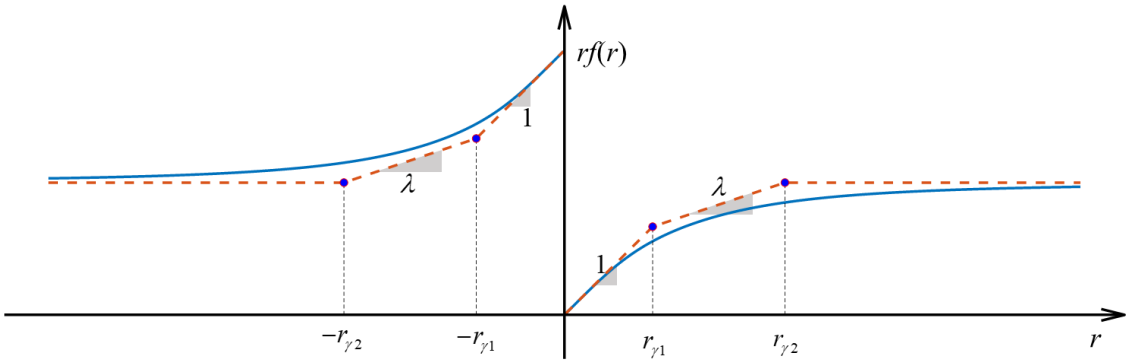

Figure 3. Function used for modelling radial distortion in fish-eye lenses.

An interesting property of this distortion function is that it includes a continuation between $r\rightarrow\infty$ and $r\rightarrow$ -∞, i.e. when Z_c changes sign from positive to negative. In fact, it may happen that for strong fish-eye lens distortion some points closer to the camera eye have a $Z_c < 0$, which consists in an equivalent field of view, i.e. the field of view with

respect to the equivalent pinhole, slightly higher than 180°. Without this continuation, points beyond the standard 180° field of view may remain uncovered by the model, even if within the camera frame. In the distortion function, the problem is treated as for spherical distortion lenses, i.e. there is an axial symmetry between what happens for $r > 0$ and what happens for $r < 0$.

The solution of the integral in (3) is shown below for the sake of completeness

$$\int_0^t \frac{1}{1+\tau^{n/2}}\,d\tau = \begin{cases} 2\left[\sqrt{t} + \log\left(\frac{1}{1+\sqrt{t}}\right)\right] & n=1 \\ \frac{2}{n}\sum_{k=0}^{n-1} c_{k,n}^2 \log\left(\frac{c_{k,n}}{c_{k,n}-\sqrt{t}}\right) & n>1 \end{cases}, \qquad c_{k,n} = \exp\left(j\frac{2k+1}{n}\pi\right) \quad (4)$$

where j is the imaginary unit. Two particular cases, for $n = 2$ and $n = 4$, are shown below:

$$G_2(t) = \int_0^t \frac{1}{1+\tau}\,d\tau = \log(1+t) \quad (5a)$$

$$G_4(t) = \int_0^t \frac{1}{1+\tau^2}\,d\tau = \operatorname{atan}(t) \quad (5b)$$

The first case in (5a) is compatible with the model defined as fisheye transform [Hughes 2008], while the second case in (5b) is compatible with the models defined as perspective model and field-of-view model [Hughes 2008].

III.C TANGENTIAL AND PRISM DISTORTION

The tangential-prism distortion component used in this paper is given by

$$\boldsymbol{K}_{tp}(\boldsymbol{P}_c) = \operatorname{diag}\left(\frac{2X_c\boldsymbol{P}_c\boldsymbol{k}_t^T + k_{tpx}R_c^2}{X_c\left(Z_c - 2\boldsymbol{P}_c\boldsymbol{k}_t^T\right) - k_{tpx}R_c^2}, \frac{2Y_c\boldsymbol{P}_c\boldsymbol{k}_t^T + k_{tpy}R_c^2}{Y_c\left(Z_c - 2\boldsymbol{P}_c\boldsymbol{k}_t^T\right) - k_{tpy}R_c^2}, 0\right) \quad (6)$$

where $\boldsymbol{k}_t$ = [k_{tx}, k_{ty}, 0] is the vector containing the tangential distortion coefficients, $k_{tpx} = k_{tx} + k_{px}$ and $k_{tpy} = k_{ty} + k_{py}$, with $\boldsymbol{k}_p$ = [k_{px}, k_{py}, 0] containing the prism distortion coefficients.

Note that the tangential-prism distortion matrix in (6), when the distortion parameters are very small, reduces to:

$$\boldsymbol{K}_{tp}\left(\boldsymbol{P}_c\right) \cong \operatorname{diag}\left(\frac{2X_c\boldsymbol{P}_c\boldsymbol{k}_t^T + k_{tpx}R_c^2}{X_cZ_c}, \frac{2Y_c\boldsymbol{P}_c\boldsymbol{k}_t^T + k_{tpy}R_c^2}{Y_cZ_c}, 0\right) \tag{7}$$

which is consistent with the model described in [Wang 2008].

III.D OPTIMIZATION

The spatial calibration process consists normally of two main phases, one related with the optimization of intrinsic and distortion parameters of the camera, one related with the optimization of the extrinsic parameters (camera position and orientation).

For the first calibration phase, multiple views of a checkerboard-like-object (see Figure 4a-b) have been collected before the experimental campaign. In order to obtain the checkerboard images, the second layer of a two-layer metal checkerboard were heated up by electrical heating stripes. A set of corner points were automatically detected from each checkerboard image, related with the reference chessboard, and used for the calibration of intrinsic and distortion parameters. In this procedure, the intrinsic parameters matrix is first initialized without including the distortion model by computing the homographies as proposed in [Zhang 2000]. After this, the radial distortion is included in the model and optimized iteratively together with the intrinsic matrix, increasing at each step the parameter *n*. The radial distortion model, which best fits in the least square sense the projection of checkerboard corners onto checkerboard images, is chosen. A final correction of the parameters is done after adding tangential and prism distortion. If these

distortion parameters do not improve the fitting, then these parameters are discarded, i.e. they are set to zero.

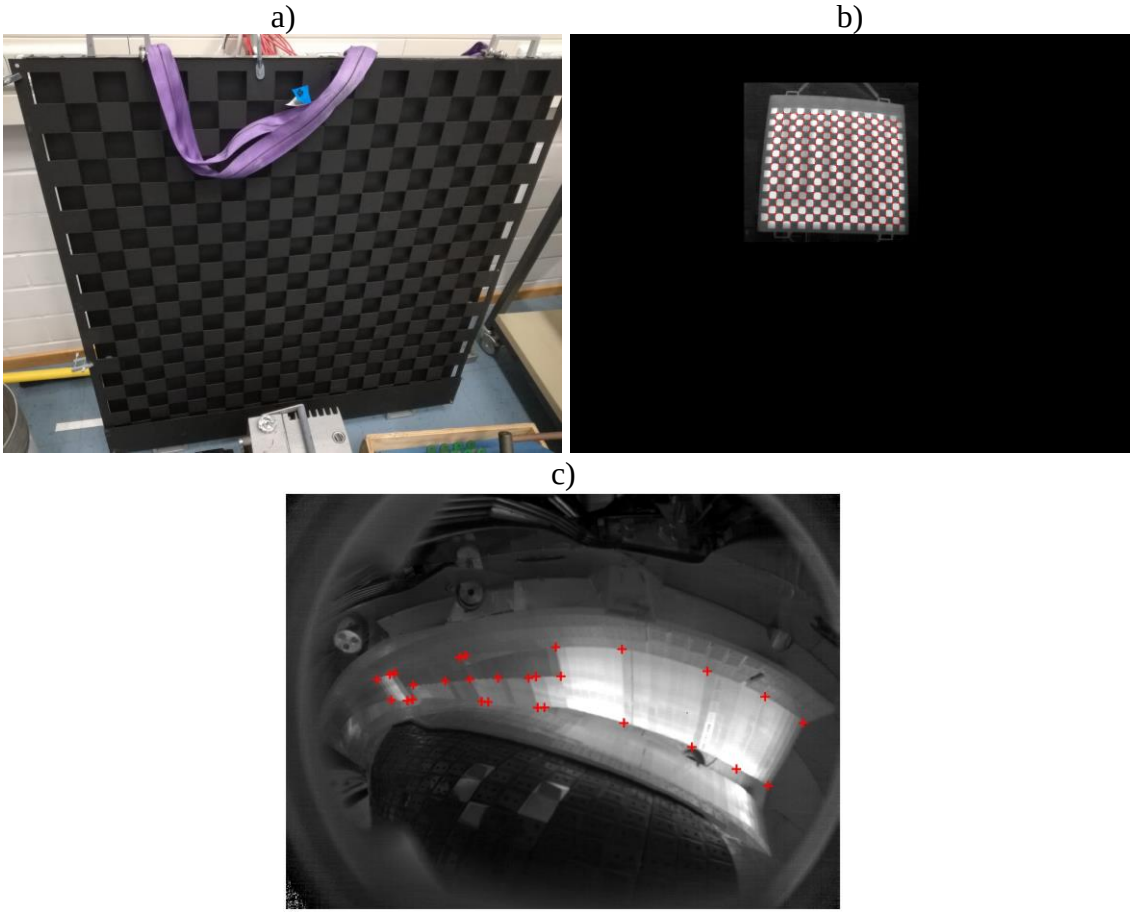

Figure 4 a) Two-layer checkerboard used to generate checkerboard images; b) Example of checkerboard image with detected corner points; c) Example of background image with selected control points.

For the second phase, a background image (see Figure 4c) is collected at the beginning of the experimental campaign, or each time the camera moves, due to maintenance or vibrations, and used to collect a set of control points on the observed surface. Normally, these points consist of the corners of the PFC tiles. The control points are related to the correspondent 3D point in a simplified CAD model of the PFCs and used for the calibration of extrinsic parameters. In this procedure, the extrinsic parameters are first initialized by considering the nominal position and orientation of the camera.

Then, the extrinsic parameters of the full camera model, which comprises also the intrinsic and distortion parameters optimized in the previous phase, are optimized in order to best fit in the least square sense the projection of 3D CAD points onto the background image.

IV. MAPPING TOOLS

Knowing the relationship between the 3D world and the camera pixels is important in thermography, since the relationship between surface temperatures observed by IR cameras and their digital levels depends on the observed materials and on camera position and orientation. It is therefore important to build a correspondence between the camera images and the corresponding thermal events, and a model of the 3D observed surface. By means of spatial calibration, explained in the previous section, it is possible to carry out this task applying proper mapping tools which can be subdivided by camera-dependent and CAD-dependent.

Scene models are an example of camera-dependent mapping tools, as they contain a pixel-based segmentation of the field of view for each camera, giving information about material and spatial properties of the target surfaces. The so-called thermal map is an example of a CAD-dependent mapping tool, since it helps to visualize all the thermal events into a common map bypassing the camera position dependence of scene models.

IV.A CAMERA-DEPENDENT: SCENE MODELING

A scene model contains, for each camera, a pixel-wise information about: the observed PFC and its emissivity properties; the distance of the target material from the camera eye and the angle of the line of sight with respect to the surface normal; the 3D coordinates of the observed target [Puig Sitjes 2018] [Puig Sitjes 2019]. It contains also

a simulation of the CAD view as it would be projected onto the camera plane, as it can be seen in Figure 5a. The overlapping of the thermal image onto the CAD view (Figure 5b) is used during experiments to help the visualization and detection of thermal events with respect to the observed surfaces.

a) b)

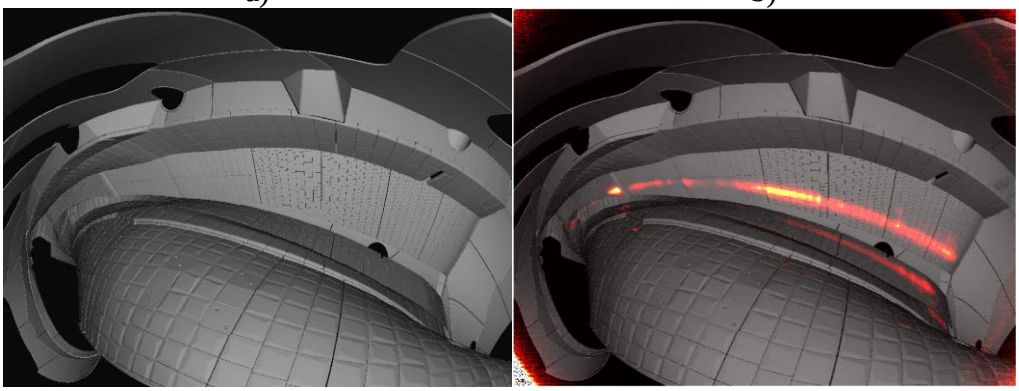

Figure 5 Scene model example. a) CAD view; b) Overlay of the camera image on the CAD view.

IV.B CAD-DEPENDENT: THERMAL MAP

A thermal map is a CAD-based 2D map which unfolds the first wall of the stellarator, including all the PFCs. By means of this map, all the thermal events taken from different cameras can be projected in one single standard grid for monitoring during experiments. The first step for the creation of the thermal map is a transformation from cartesian (Figure 6a) to helical (Figure 6b) coordinates of the stellarator inner surface, by unfolding it with respect to a helical axis and a torsion in the poloidal direction ϑ. Both helical axis and torsion angle change depending on the cross section, i.e. with respect to the toroidal angle φ.

After this change of coordinates, for each couple of coordinates φ and ϑ, a couple of new coordinates u, v is defined, obtaining the thermal map shown in Figure 7a. The coordinates u and v are obtained by line-integrating the surface along the φ and ϑ axes. Figure 7b shows an example of thermal events projected on the thermal map. Given the

fact that the torsion angle performs a rotation of 180° within each module, lower and upper divertors in module 2 and 4 of the thermal map are inverted, i.e. the lower (upper) divertor in module 2 and 4 appears on the top (bottom) of the thermal map.

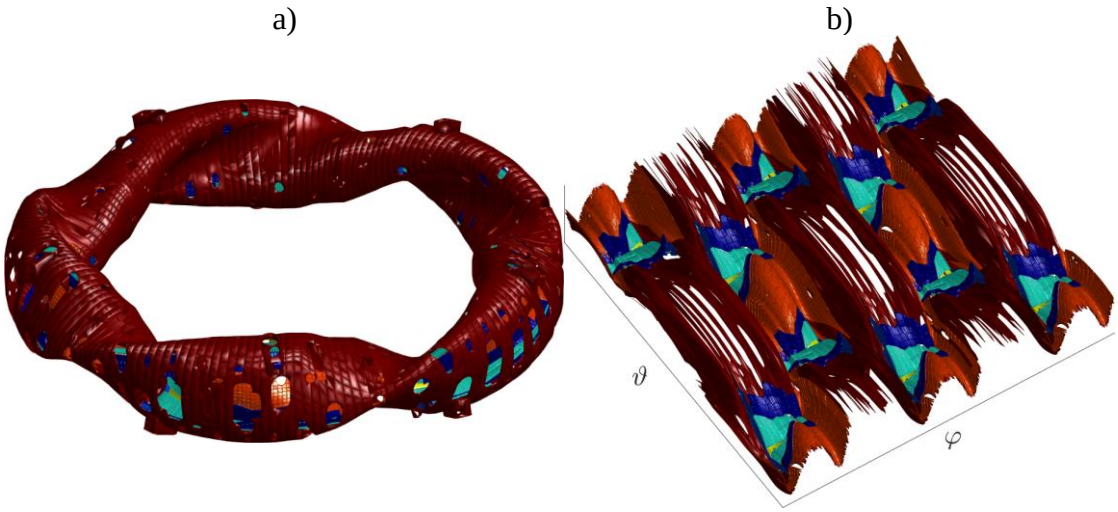

Figure 6 CAD model of the stellarator PFCs in a) cartesian coordinates and b) helical coordinates.

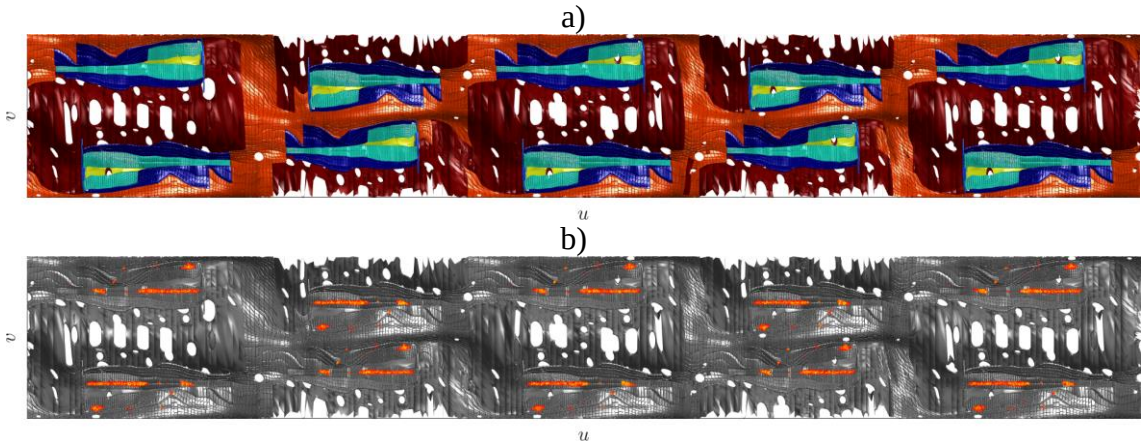

Figure 7 a) Thermal map with different PFCs highlighted with different colors. In order of appearance in the top side (bottom side) from left to right: upper (lower) divertor of module 1, lower (upper) divertor of module 2, upper (lower) divertor of module 3, lower (upper) divertor of module 4, upper (lower) divertor of module 5. b) Example of thermal events projected on the thermal map.

V. APPLICATIONS

These mapping tools are really important since they connect the information in

the camera images with the actual observed structures. In this way, it is possible to describe all the thermal events not only in the image coordinate system, but also on the complex 3D structure of the stellarator, giving useful 3D informations about the thermal objects detected in the images [Puig Sitjes 2019]. The detected thermal events include strike-lines, leading edges, overload hot spots, shine-through hot spots due to the heating systems, fast particle losses and surface layers.

When analysing IR data, thermal events must be identified and characterized extracting a set of significant properties. These properties or features should be usable for future offline analysis, including relating them with magnetic configurations and experimental plasma parameters, and usable online in case of dangerous events to automatically implement the proper control strategies. Thus, it is necessary to implement image processing routines to segment IR images, i.e. isolate the different thermal events with respect to image background and noise and evaluate their properties.

Some preliminary results are reported below, regarding the strike-line segmentation and characterization starting from heat-flux images.

V.A STRIKE-LINE CHARACTERIZATION

Figure 8a shows the heat-flux distribution in one of the ten divertors of W7-X. The heat-flux image is obtained by aligning the heat-flux profiles, defined as described in [Gao 2019], next to each other in a picture. Each vertical line in the heat-flux image corresponds to a single profile. As a first attempt of isolating the strike-line and removing the effect of noise, hot spots and leading edges, a spatio-temporal prefiltering is applied to the image. This prefiltering stage, performed by means of a gaussian spatial filter and of a moving average filter in the time dimension, helps avoiding an “object” fragmentation when segmenting the strike-line. The result is shown in Figure 8b. After this prefiltering stage, for each profile, i.e. each vertical line in the image, of the divertor

target (horizontal or vertical), the strike-line width is estimated, adapting the formula of the wetted area proposed in [Jakubowski 2018b].

At the end of the process, in standard magnetic configuration [Andreeva 2002] it is possible to identify three main objects in the final image (see Figure 8c). These three objects can be analysed and characterized by means of spatial and thermal features and used to give a general characterization of the strike-line in this particular magnetic configuration.

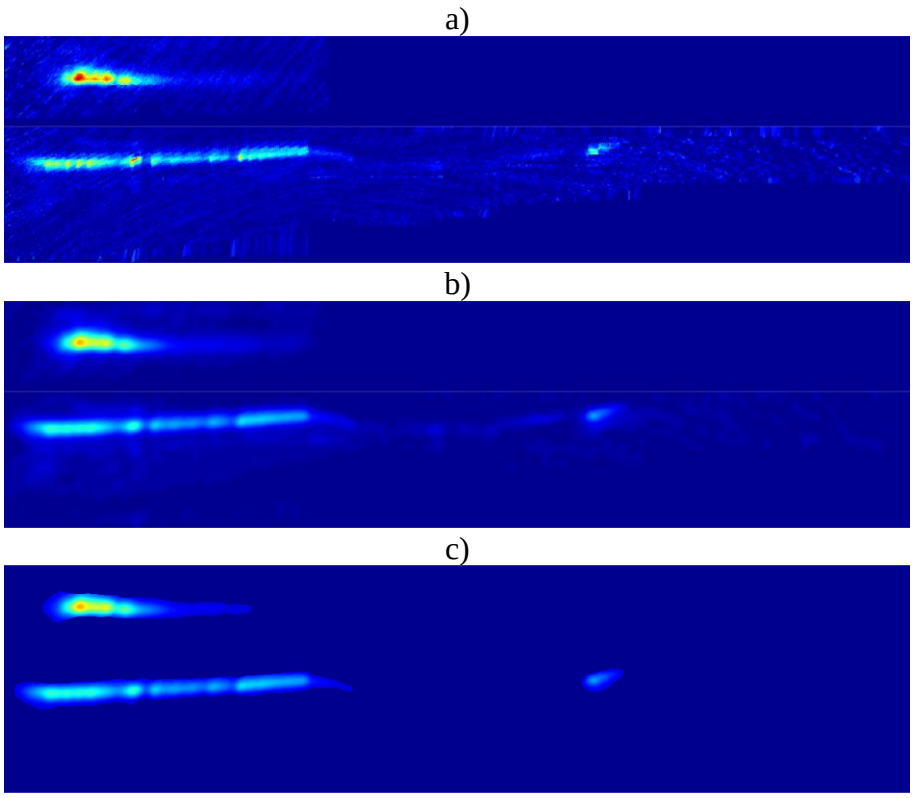

Figure 8. a) Original heat-flux image, b) prefiltered image, c) segmented image.

VI. CONCLUSIONS

In this paper an overview of the tools under development at W7-X for the interpretation and analysis of thermographic images is presented. These tools help to give a meaning to the raw data coming from IR cameras, transforming them into temperatures and heat fluxes and connecting them to the 3D position of the target surfaces. These relationships are relevant when designing real time systems for PFC protection, since they

help to save, only periodically, the information needed for real time calculations. A lot of work needs to be done in order to automate the procedures in case of camera movements or vibrations, which are very likely during next operation of W7-X, but a whole range of possibilities is now open for the analysis of thermographic data. In this context, are included: the characterisation of the heat loads on the PFC targets; the study of their relationship with experimental parameters; their monitoring and control for PFC protection.

ACKNOWLEDGMENTS

This work has been carried out within the framework of the EUROfusion Consortium and has received funding from the Euratom research and training programme 2014-2018 and 2019-2020 under grant agreement No 633053. The views and opinions expressed herein do not necessarily reflect those of the European Commission.

DECLARATION OF INTEREST STATEMENT

The authors confirm that there are no known conflicts of interest associated with this publication and there has been no significant financial support for this work that could have influenced its outcome.

REFERENCES

[Sunn Pedersen 2019] T. Sunn Pedersen *et al.*, "First divertor physics studies in Wendelstein 7-X", Nuclear Fusion, vol. 59 (9), 096014 (2019).

[Puig Sitjes 2018] A. Puig Sitjes, M. Jakubowski, A. Ali, P. Drewelow, V. Moncada, F. Pisano, T. T. Ngo, B. Cannas, J. M. Travere, G. Kocsis, T. Szepesi, T. Szabolics & W7-X Team, "Wendelstein 7-X Near Real-Time Image Diagnostic System for Plasma-Facing

Components Protection", *Fusion Science and Technology*, vol. 74 (1-2), 116-124 (2018).

[Puig Sitjes 2019] A. Puig Sitjes, Y. Gao, M. Jakubowski, P. Drewelow, H. Niemann, A. Ali, V. Moncada, F. Pisano, T. T. Ngo, B. Cannas, M. Sleczka and W7-X Team, "Observation of thermal events on the plasma facing components of Wendelstein 7-X", 3rd European Conference on Plasma Diagnostics, 6th-9th May 2019, Lisbon, Portugal

[Jakubowski 2018] M. Jakubowski, P. Drewelow, J. Fellinger, A. Puig Sitjes, G. Wurden, A. Ali, C. Biedermann, B. Cannas, D. Chauvin, M. Gamradt, H. Greve, Y. Gao, D. Hathiramani, R. König, A. Lorenz, V. Moncada, H. Niemann, T. T. Ngo, F. Pisano, T. Sunn Pedersen, and W7-X Team, "Infrared imaging systems for wall protection in the W7-X stellarator", Review of Scientific Instruments, vol. 89 (10), 10E116 (2018).

[Gao 2019] Y. Gao, M. W. Jakubowski, P. Drewelow, F. Pisano, A. Puig Sitjes, H. Niemann, A. Ali, B. Cannas and W7-X Team, "Methods for quantitative study of divertor heat loads on W7-X", Nuclear Fusion, vol. 59 (6), 066007 (2019).

[Forsyth 2003] D. A. Forsyth and J. Ponce, Computer Vision, a Modern Approach (Prentice Hall, 2003).

[Sturm 2016] P. Sturm, "Pinhole camera model," in Computer Vision, edited by K. Ikeuchi (Springer Science+Business Media, New York, 2016), Vol. 2014, pp. 610–613.

[Pisano 2018] F. Pisano, B. Cannas, M. W. Jakubowski, H. Niemann, A. Puig

Sitjes, G. A. Wurden and W7-X Team, “Towards a new image processing system at Wendelstein 7-X: From spatial calibration to characterization of thermal events”, *Review of Scientific Instruments*, vol. 89 (12), 123503 (2018).

[Hughes 2008] C. Hughes, M. Glavin, E. Jones, P. Denny, “Review of Geometric Distortion Compensation in Fish-Eye Cameras”, *IET Irish Signals and Systems Conference (ISSC 2008)*, Galway, 2008, pp. 162-167.

[Wang 2008] J. Wang, F. Shi, J. Zhang, Y. Liu, “A new calibration model of camera lens distortion”, *Pattern Recognition*, vol. 41, pp. 607-615 (2008).

[Zhang 2000] *Z*. Zhang, “A flexible new technique for camera calibration,” *IEEE Trans. Pattern Anal. Mach. Intell.*, vol. 22(11), 1330–1334 (2000).

[Jakubowski 2018b] M. W. Jakubowski, A. Ali, P. Drewelow, Y. Gao, K. Hammond, H. Niemann, A. Puig Sitjes, F. Pisano, M. Ślęczka, S. Brezinsek, B. Cannas, M. Endler, R. König, M. Otte, T. S. Pedersen, G. Wurden, D. Zhang and W7-X Team, “3D Heat and Particle Fluxes in Wendelstein 7-X”, 27th IAEA Fusion Energy Conference (FEC 2018), Gandhinagar.

[Andreeva 2002] T. Andreeva, J. Kisslinger, H. Wobig, “Characteristics of main configurations of Wendelstein 7-X”, Problems of Atomic Science and Technology Series: Plasma Physics, vol. 4, pp. 45-47 (2002).